APRICOT CAKE EXTRACT AS CORROSION INHIBITOR OF STEEL: CHEMICAL COMPOSITION AND ANTI-CORROSION PROPERTIES

Viktoria Vorobyova [a*], Margarita Skiba [b]

[a]National Technical University of Ukraine "Igor Sikorsky Kyiv Polytechnic Institute",
37, Peremohy ave., Kiev 03056, Ukraine
[b]Ukrainian State University of Chemical Technology, 8, Gagarina ave., Dnipro 49005, Ukraine
[*]e-mail: vorobyovavika1988@gmail.com

Abstract. The protection performance of self-assembled layers (SALs) formed by apricot cake extract (ACE) on the surface of steel has been studied. Characterization of the apricot cake extract was carried out using the gas chromatography-mass spectrometry analysis. The anti-corrosion effect of the self-assembled layers was determined by weight loss experiments, scanning electron microscopy and electrochemical methods. It was revealed that the protection ability of the SALs is determined by the time of film formation on the steel surface. The maximal corrosion inhibition efficiency (about 93%) was obtained after 48 h process of film formation in the vapour phase of the apricot cake extract. The results of the polarization test revealed that the ACE acted as a mixed type inhibitor and retarded both anodic and cathodic reactions rates. The results of the electrochemical analysis revealed that the ACE modified steel showed better corrosion protection in conditions of periodic condensation of moisture.

Keywords: apricot cake extract, self-assembled layer, green corrosion inhibitor, steel, organic coating.

Introduction

Surface modification by self-assembled layers (SALs) of vapour phase corrosion inhibitor currently attracts considerable attention due to its potential application in anticorrosive protection [1]. The SAL forms a robust barrier film between the metal and corrosive media, thus controlling the penetration of corrosive agents into the metal surface [2-6]. Self-assembled monolayers (SAM) of organic molecules are among the most versatile inhibitors to impede the corrosion of steel by forming a very thin, dense and protective layer at the surface of the metal. Their relatively good protection efficiency, their ease of application, especially on very complicated shaped objects, as well as their nanometric thickness have turned them into attractive candidates for protection of metallic surfaces. Compared with the traditional corrosion inhibition techniques, SALs have been extensively studied due to a lower dosage, higher coverage, fewer defects, and higher inhibition efficiency.

Numerous organic compounds such as urea-amine compounds, monoterpenoid phenols, alkanoic and phosphonic acid derivatives, thiol and some other heterocyclic compounds containing heteroatoms, such as sulphur and nitrogen have been employed as self-assembled adsorptive inhibitors for metal corrosion [1-10]. It was found that monoterpenoid phenols SAM protect steel from corrosion [11]. However, some synthetic compounds may result in environmental pollution, and increase human health risk. Recently, attention has been turned to exploring cheap, biodegradable, and environmentally-friendly corrosion inhibitors with excellent effect [11-16]. The term "green inhibitor" or "eco-friendly inhibitor" refers to substances that are biocompatible, such as plant extracts, since they are of biological origin. Plant extracts, which are natural products, are easily available, renewable, non-toxic, and inexpensive. However, only a few reports described an inhibitor extracted from a waste without harm to plants and environment. Therefore, it is an interesting and useful task to find new sources for highlighting anticorrosive active compounds and to obtain organic compounds for their further use as self-assembled layers.

Several studies have suggested that inhibition efficiency could be improved by using mixtures of inhibitors with respect to a single inhibitor [19,20]. It means that the extract of a plant raw material, which is a mix of components, can be used as self-assembled layers for corrosion

inhibition of steel. It is known that apricot processing by-products are a source of functional compounds and can be used for corrosion inhibition of steel. Apricot fruits (*Prunus Armeniaca L.*) are valued and highly consumed all over the world, both for their flavour and for nutritional qualities. Ukraine is one of the major apricot producers in the world with the approximate annual yield of 160 000 tonnes/year of fresh fruit, seeds, and kernels, respectively. About 20% of the harvest turns into waste from processing of this raw material. The successful utilization of this natural waste may also provide an option for resource recovery. The cake of apricot can be used to obtain volatile corrosion inhibitors that form self-assembled monolayers. In the literature, one can also find no information about possible applications of apricot cakes and its extracted compounds for the development of self-assembly vapour phase corrosion inhibitor for mild steel.

The aim of the present work is to evaluate the corrosion inhibition effect of apricot cake extract (ACE) as "green" self-assembly vapour phase inhibitor of steel corrosion. The organic compounds present in the apricot cake extract were characterized by gas chromatography-mass spectrometry. The SAL modified steel surface was characterized by scanning electron microscope and atomic force microscopy. The corrosion inhibition efficiency of the apricot cake extract was characterized by using electrochemical methods and was compared to their inhibition activity evaluated by the method of accelerated tests under simulated operational conditions. The inhibition performance and mechanism were also discussed. Furthermore, it is necessary to estimate the contributions of the main compounds to the inhibition effect and model the adsorption of the main components on the MS surface, which can also illustrate the experimental results.

Experimental
Materials

The apricot (*Prunus Armeniaca* L.) cultivar known under local name "Favorite" were harvested (during July 2018) in two geographical regions of Ukraine (Kherson, Nikolaev). The apricot cake was supplied by an agro-food company (Vinni Frut) from the Vinnytsia city, Ukraine.

Corrosion test samples (electrodes) were manufactured from mild steel St37-2. The mild steel (DIN 17100 R St 37-2) were purchased from Rocholl (Aglasterhausen, Germany). The mild steel strips with the chemical composition 0.20%

C, 0.43% Mn, 0.55% Si, 0.016% S, 0.02% P and Fe balanced were used for the corrosion tests and electrochemical measurements [21].

Preparation and characterization of the apricot cake extract

The apricot press cake was obtained by cold pressing. The apricot press cake extract was obtained with a 2-propanol/ethanol solution (v:v= 50:50) in a Soxhlet apparatus. The solvent was removed at 40°C in a rotary vacuum evaporator under a nitrogen stream. Finally, the obtained extract was dissolved in 2-propanol in different concentrations. The prepared solution was used as self-assembly vapour phase inhibitor of steel corrosion.

Pretreatment of steel electrode and self-assembly film formation

The steel electrode was polished with various grades of sandpaper and then sonicated in deionized water, followed by ethanol, and eventually dried in a vacuum oven. The self-assembly films of ACE were prepared in vapour phase at 22°C (spontaneous volatilization). For the formation of a self-assembly films, cleaned steel samples were suspended in a 250 mL conical flask with a tight-fitting rubber containing a small dish with ACE (2 mL). The ACE was placed in a dish for a certain period of time (depending on the experiment from 12 to 72 h) to form the self-assembled films. After surface modification, the SAM vapour phase of volatile compounds of ACE was sampled.

Gas chromatography-mass spectrometry analysis

The composition of volatile substances of the extract was identified by *gas chromatography coupled to mass spectrometry* (GC-MS). A Shimadzu gas chromatograph (model GC 17A) equipped with flame ionization detector, was operated under the following conditions: capillary fused silica column (CBP-5) (length, 25 m; internal diameter, 0.25 mm; film thickness, 0.22 μm), ion source temperature of 280°C. The GC-MS was operated in the electron impact ionization mode at 70 eV. The oven temperature was set as follows: the initial temperature of 50°C was maintained for 2 min, and then increased to 200°C at the rate of 10°C/min and held for 5 min. Afterwards the temperature was ramped to 250°C at a rate of 25°C/min (for 15 min). Other operating conditions were as follows: gas carrier He (99.99%), inlet pressure of 76 kPa with a linear velocity of 20 cm/s; injector temperature of 250°C; detector temperature of 310°C; 1:25 split ratio. The relative contents of the chemical components of the extract were found using the method of internal normalization of the areas of

peaks without correcting the sensitivity coefficients. The percentage of each compound was determined from its peak area and the sum of the areas of all peaks detected in the total ion current trace. The identification and quantification of the components was carried out by using a commercially available databases were also used: NIST 05 (National Institute of Standards and Technology, USA) and Mass Finder3 (Dr. Hochmut, Scientific Consulting, Germany). If only one identification method resulted in a match (MS), the identification was defined as "tentative". Mass spectra of all detected compounds were compared with those of standard compounds. Data were processed using the AMDIS software [22-24].

Corrosion inhibition efficiency characterization

The surface morphology and coating were examined by *scanning electron microscope* (SEM) FEI E-SEM XL 30 (Detection of secondary electrons). For SEM images, an area of 1 cm^2 of sample was taken.

Surface analysis was carried out by the *atomic force microscopy* (AFM) technique in order to evaluate the surface morphology of the steel samples after 48 and 72 h of film-forming in the vapour phase of inhibitors. Samples of dimension 1.0×1.0×0.06 cm were abraded with emery paper (grade 320-500-800) and then washed with distilled water and acetone. The surface morphology and coating was analysed with the help of unit atomic force microscope SPA-400 SPM. All images were processed and the corresponding roughness calculated using either Gwyddion or WSxM software [25].

Gravimetric measurements

Inhibitor effectiveness of the apricot cake extract as a vapour phase inhibitor of atmospheric corrosion of steel was evaluated with the method of accelerated tests under the condition of condensation of moisture. The final geometrical area was 25 cm^2. The gravimetric measurement was conducted by suspending the samples in a 250 mL conical flask with a tight-fitting rubber cork containing a small dish. The vapour phase corrosion inhibitor samples were placed in the dish (2 mL) for a certain period of time (depending on the experiment, from 24 to 72 h) to form a protective film. After the film-forming period in the vapour phase of the apricot cake extract, 15 mL of deionized water was added. The test process included cyclic warming and cooling of the samples in a corrosion testing chamber with varying humidity. One cycle included an 8 h exposure in the thermostat (40±1°C), and a 16 h exposure at room temperature 25°C). The total

duration of the test was set to 21 days. The gravimetric measurements were repeated twice. The inhibition efficiency (*IE*, %) was estimated according to the degree of protection against corrosion [11-15].

$$CR = \frac{W_0 - W_1}{A \times \tau} \qquad (1)$$

$$IE = \frac{CR_1 - CR_2}{CR_1} \times 100 \qquad (2)$$

where, *CR*- the corrosion rate, g m^{-2} h^{-1};
  A- the sample area, m^2;
  W$_0$- the initial weight of the sample, g;
  W$_1$- the sample weight after the immersion time, g;
  τ- the immersion time, h;
  CR$_1$, and *CR$_2$*- the corrosion rates without and with the inhibitor, g m^{-2} h^{-1}.

Electrochemical measurements

The electrochemical measurements were conducted in a simulated atmospheric corrosion solution (0.5 M Na$_2$SO$_4$, pH 7.2) [26]. Electrochemical experiments were carried out in a conventional three-electrode cell with a platinum counter electrode and a saturated calomel electrode (*SCE*) coupled to a fine Luggin capillary as the reference electrode. To minimize the ohmic contribution, the tip of the Luggin capillary was kept close to the working electrode. The carbon steel working electrode was designed with a fixed exposed surface area of 0.385 cm^2. As a specific feature of our electrochemical measurements, we can mention the following fact: the disk-shaped surface of the end face of the working electrode was immersed in surface layers of the working solution by at most 1-2 mm [1,27]. This enabled us to perform more exact modeling of the atmospheric corrosion running on the metal surface in thin layers of condensed moisture. A capillary from the reference electrode was placed near the surface of the working electrode from below. A potential scanning rate was 0.5 mV/s; anodic and cathodic polarization was performed in the range ±300 mV from the free corrosion potential. Current-potential dependences were measured five times to ensure results convergence. Samples for electrochemical studies were prepared similarly to the methods described in the paragraph above.

Results and discussion
The apricot cake extract characterization

The plant extract is a mixture of various components which cause a formation of the

self-assembling layers on the surface of the steel. The inhibition performances of the apricot cake extract (ACE) are closely related to the presence of complex organic compounds in its composition. It is difficult to define which components of the apricot cake extract are adsorbed on the steel surface and provide the inhibition effectiveness. Therefore, the extract from apricot cake was analyzed by gas chromatography-mass spectroscopy. The obtained results of ACE in 2-propanol are presented in Figure 1 and Table 1. Individual peaks were identified by comparing their retention indices (RI) and mass spectra (MS) with spectra in commercial library and comparison of the mass spectra with literature data. Spectra and RI values were compared with those of authentic compounds commercially obtained.

As a result of the GC-MS analysis, 39 phytochemical compounds were identified in the apricot cake extract. The main components are aldehydes: hexanal (1.32%), (*E*)-2-hexanal (3.10%), (*Z*)-2-heptenal (3.65%), heptanal (2.18%), 2-phenylacetaaldehyde (1.29%), *β*-cyclocitral (5.17%), (*E,E*)-2,4-decadienal (3.65%), also ketones: 2-hexanone (1.03%), 3-hexanone (0.54%). The class of alcohols is presented by (*Z*)-3-hexenol (0.76%), (*E*)-2-hexenol (1.87%), hexanol (5.67%). Additionally, the extract contains esters, such as (*E*)-2-hexenyl acetate (2.78%), (*Z*)-3-hexenyl butanoate (1.51%), hexyl hexanoate (2.12%), in a minor amount. Also, the apricot cake extract contains many acids, this class is represented by octadecanoic acid (6.02%), (*9Z,12Z*)-octadeca-9,12-dienoic acid (4.2%), hexadecanoic acid (5.4%), (*9Z*)-octadec-9-enoic acid (6.1%), (*9Z,12Z,15Z*)-9,12,15-octadecatrienoic acid (0.63%). The extract of apricot cake contains an increased content of terpene alcohols: linalool (3.06%), *α*-terpineol (5.98%), nerol (3.02%), geraniol (8.54%), isoborneol (1.03%), nerolidol (8.54%), farnesol (1.38%) and others. These compounds represented over 18% of the total volatiles in the apricot cake.
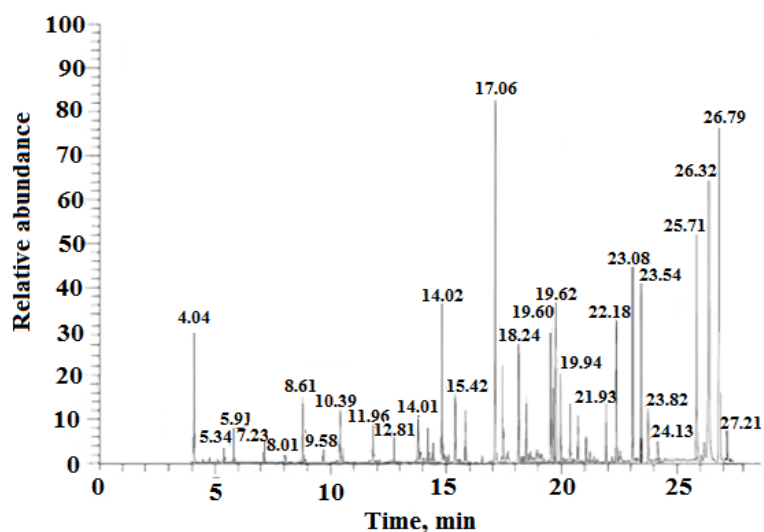

Figure 1. GC-MS spectral chromatogram of apricot cake extract.

Table 1

Component composition of volatile substances of extracts squeezes of apricot.

Retention time, min	Name of the compound	Molecular formula	Molecular weight, g mol^{-1}	Quantitative ratio, %
4.04	hexanol	$C_6H_{14}O$	102	5.67
5.34	(*Z*)-3-hexenol	$C_6H_{12}O$	100	0.76
5.91	(*E*)-2-hexenol	$C_6H_{12}O$	100	1.87
7.23	2-hexanone	$C_6H_{12}O$	100	1.03
8.01	3-hexanone	$C_6H_{12}O$	100	0.54
8.61	(*Z*)-2-heptenal	$C_7H_{12}O$	112	3.65
9.58	hexanal	$C_6H_{12}O$	100	1.32
10.06	benzaldehyde	C_7H_6O	106	1.94
10.39	(*E*)-2-hexanal	$C_6H_{12}O$	98	3.10
11.96	heptanal	$C_7H_{14}O$	114	2.18
12.71	2-phenylacetaldehyde	C_8H_8O	120	1.29

Retention time, min	Name of the compound	Molecular formula	Molecular weight, g mol^{-1}	Quantitative ratio, %
14.01	(*E*)-2-hexenyl acetate	C$_8$H$_{14}$O$_2$	142	2.78
14.37	5-butyloxolan-2-one (*γ*-octalactone)	C$_8$H$_{14}$O$_2$	142	2.03
14.41	phenol, 5-methyl-2-(1-methylethyl)-	C$_{10}$H$_{14}$O	150	4.58
14.43	endo-1,7,7-trimethyl- bicyclo[2.2.1]heptan-2-ol (isoborneol)	C$_{10}$H$_{18}$O	154	1.03
14.92	2,6,6-trimethylcyclohexene-1-carbaldehyde (*β*-cyclocitral)	C$_{10}$H$_{16}$O	152	5.17
15.42	(2*E*,4*E*)-deca-2,4-dienal	C$_{10}$H$_{16}$O	152	2.65
15.86	(*Z*)-3,7-dimethyl-2,6-octadien-1-ol (nerol)	C$_1$$_0H_{18}$O	154	3.02
16.74	(9*Z*,12*Z*,15*Z*)-9,12,15-octadecatrienoic acid (*α*-linolenic acid)	C$_{18}$H$_{30}$O$_2$	278	0.63
17.06	(2*E*)-3,7-dimethyl-2,6-octadien-1-ol (geraniol)	C$_{10}$H$_{18}$O	154	8.54
17.29	(9*Z*,12*Z*)-octadeca-9,12-dienoic acid (linoleic acid)	C$_{18}$H$_{32}$O$_2$	280	4.20
18.24	hexadecanoicacid (palmitic acid)	C$_{16}$H$_{32}$O$_2$	256	5.40
18.32	3,7-dimethylocta-1,6-dien-3-ol (linalool)	C$_{10}$H$_{18}$O	154	3.06
19.60	octadecanoic acid (stearic acid)	C$_{18}$H$_{36}$O$_2$	284	4.02
19.62	(9*Z*)-octadec-9-enoic acid	C$_{18}$H$_{34}$O$_2$	182	6.10
19.94	5-hexyloxolan-2-one (*γ*-decalactone)	C$_{10}$H$_{18}$O$_2$	170	3.65
20.67	(7aR)-5,6,7,7a-tetrahydro-4,4,7a-trimethyl-2(4H)-benzofuranone	C$_{11}$H$_{16}$O$_2$	180	2.05
20.91	5-pentyl-5-pentanolide (*δ*-decalactone)	C$_{10}$H$_{18}$O$_2$	170	2.87
21.09	(*Z*)-3-hexenyl butanoate	C$_{10}$H$_{18}$O$_2$	170	1.51
21.93	hexyl hexanoate	C$_{12}$H$_{24}$O$_2$	200	2.12
22.18	(1*R*,2*S*,6*S*,7*S*,8*S*)-8-isopropyl-1,3-dimethyltricyclo[4.4.0.0]dec-3-ene (*α*-copaene)	C$_{15}$H$_{24}$	204	4.02
23.08	3-cyclohexen-1-ol, 4-methyl-1-(1-methylethyl) (4-terpineol)	C$_{10}$H$_{18}$O	154	4.98
23.54	2-(4-methylcyclohex-3-en-1-yl)propan-2-ol (*α*-terpineol)	C$_{10}$H$_{18}$O	154	5.98
23.82	(3*E*)-4-(2,6,6-trimethylcyclohex-1-en-1-yl)but-3-en-2-one (*β*-ionone)	C$_{13}$H$_{20}$O	192	1.97
24.13	4-(2,6,6-trimethylcyclohexa-1,3-dienyl)butan-2-one (dihydro-*β*-ionone)	C$_{13}$H$_{22}$O	194	0.98
25.71	3,7-dimethyl-2,6-octadien-1-yl acetate	C$_{13}$H$_{22}$O	170	6.10
26.32	dihydro-5-octyl-2(3*H*)-furanone	C$_{12}$H$_{22}$O$_2$	198	7.65
26.79	3,7,11-trimethyl-1,6,10-dodecatrien-3-ol (nerolidol)	C$_{15}$H$_{26}$O	222	8.54
27.21	(2*E*,6*E*)-3,7,11-trimethyldodeca-2,6,10-trien-1-ol (farnesol)	C$_{15}$H$_{26}$O	222	1.38

The results of the quantitative ratio given in Table 1 show that, among the identified aldehydes, the major compounds are (*Z*)-2-heptenal, 2-phenylacetaldehyde, hexanol, (*E*)-2-hexanal, *β*-cyclocitral, nerol. The effect of 2-phenylacetaldehyde and (*E*)-2-hexanal on the corrosion behaviour of steel was studied through electrochemical techniques, and characterized by SEM and AFM [15].

Anti-corrosive effect evaluation of the apricot cake extract

Effect of apricot cake extract concentration

Table 2 represents inhibition efficiency values obtained from the weight loss in conditions of periodic condensation of moisture after a period of film-forming in the presence of different concentrations of ACE. These results demonstrate that the ACE inhibitor has a good performance on corrosion inhibition by forming a multilayer on the steel surface. Clearly, inhibition efficiency increases with an increase of the inhibitor concentration, *i.e.* the corrosion inhibition rises with the inhibitor concentration. The increase of the inhibition efficiency in the presence of the SALs shows that more ACE molecules were adsorbed on the steel surface at the higher concentration of ACE.

At 100 mg mL^{-1}, the maximum *IE* is 97.60% for apricot cake extract, which indicates that all compounds act as moderate steel corrosion inhibitors. The apricot cake extract contains many organic compounds, which not only can be adsorbed on steel surface through electrostatic interaction but also can form a strong coordination bond with iron for the existence of heteroatoms and aromatic rings. The combination of physisorption and chemisorption makes the active components of apricot cake extract be strongly adsorbed onto the steel surface, preventing the steel from corrosion [28-30].

Table 2
Calculated corrosion rates and inhibition efficiency of SALs at different ACE concentrations.

The inhibitor concentration, mg·mL^{-1}	CR, g m^{-2} h^{-1}	IE, %
10	0.1585	15.94
20	0.0912	51.46
30	0.0610	67.52
40	0.0526	71.98
50	0.0382	79.67
60	0.0306	88.90
70	0.0186	91.00
80	0.0121	93.71
100	0.0045	97.60
no inhibitor	0.1879	–

Film-forming time 48 h;
Periodic condensation of moisture for 21 days.

Effect of assembly time

Table 3 presents the results for bare steel strips and surface modified steel strips in the environment of volatile compounds of the apricot cake extract. For the steel modified by ACE for 12 h and 24 h, the corrosion rate (*CR*) values are 0.1359 g m^{-2} h^{-1} and 0.0929 g m^{-2} h^{-1} according to Eq.(1), and the inhibition efficiency (*IE*) values are 27.69 and 50.55% according to Eq.(2). While the assembly time was further extended to 40 h, the value of *CR* reached 0.0457 g m^{-2} h^{-1} and *IE* 75.64%. However, the increase of *IE* value at 60 h (92.08%) is less obvious than *IE* value at 48 h (91%) of assembly time on the modified electrode. It indicates that the ACE molecules on steel surface have attained a saturated state after the self-assembling time of 48 h. With an increase in immersion time, the film becomes denser and more stable.

Table 3
Calculated corrosion rates and inhibition efficiency of SALs at different assembly time.

Film-forming time, h	CR, g m^{-2} h^{-1}	IE, %
12	0.1359	27.69
24	0.0929	50.55
30	0.0776	58.67
35	0.0564	69.95
40	0.0457	75.64
48	0.0186	91.00
60	0.0148	92.08
72	0.0131	93.01
no inhibitor	0.1879	–

Periodic condensation of moisture for 21 days;
ACE concentration 70 mg mL^{-1}.

This result proves the formation of denser and highly organized SALs on the electrode surface after 48 h of film formation. There was no significant increase observed after 48 h of immersion time, so this time was selected for further experiments. Polarization measurements were performed to monitor the mechanism of anodic and cathodic partial reactions as well as identifying the effect of an inhibitor on each partial reaction. Polarization curves were measured after steel assembly time in the environment of volatile compounds of the apricot cake extract, in 12, 24, 48 and 72 h of exposure. The corresponding corrosion potential (E_{corr}), corrosion current density (I_{corr}), anodic Tafel slopes (b_a), and cathodic Tafel slopes (b_c) are listed in Table 4.

The cathode branches of polarization curves that characterize the relation between the reaction rate of $O_2 + H_2O + 4\bar{e} \rightarrow 4OH^-$ and the electrode potential drift to the area of more positive potentials (*E*) with the increasing polarization are presented in Figure 2. The anode branches that characterize the relation of the metal ionization rate to the metal potential drift to the domain of more positive values of *E*. The intersection of these branches is attained at metal corrosion potential (E_{corr}), when the cathode and the anode process reach the same rate. The free corrosion potential shifts to more positive values. In analyzing the influence of films on the rate of the partial electrode processes of anodic oxidation of steel and cathodic reduction of the molecular atmospheric oxygen in a 0.5 M Na$_2$SO$_4$ solution with and without protective films, it was discovered that, independently of the fact whether the films are present or absent on the steel surface, the rate of cathodic processes is much higher than the rate of anodic processes (Figure 2).

The anodic and cathodic corrosion current density curves in presence of SALs on the surface are shifted towards lower current density region as compared to the blank. Compared with the steel without protective films, lower corrosion current density (I_{corr}) values are obtained for the SAM covered steel in 0.5 M Na$_2$SO$_4$ solutions as shown in Table 4. ACE SAL formed on the steel surface acts as a barrier to the diffusion of oxygen molecules from the solution to the steel surface, thereby resisting the transfer of oxygen to the cathodic sites of the steel surface. These dependences of the current density on the electrode potentials indicate the presence of fairly complicated multi-stage processes under the conditions of cathodic and anodic polarization of steel. The anodic curve for the steel electrode in

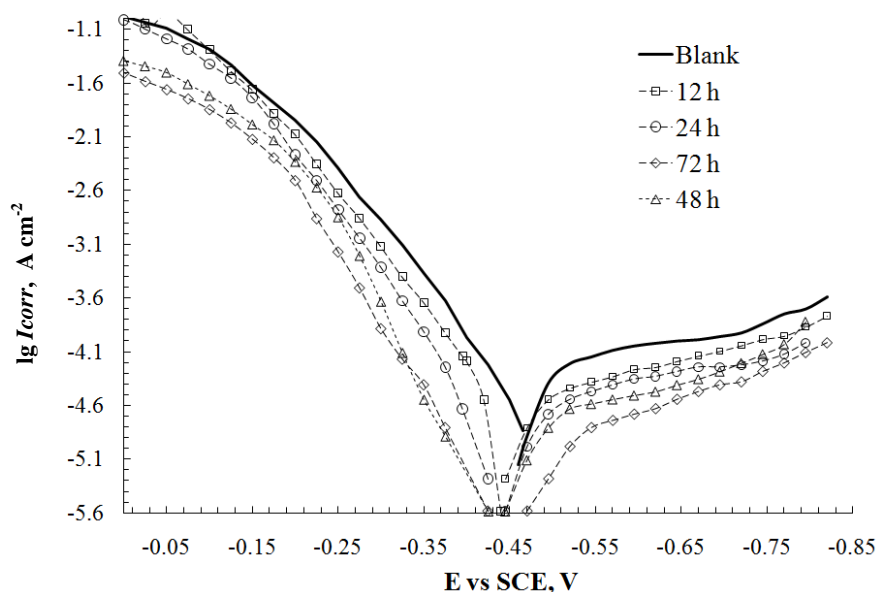simulated atmospheric corrosion water (0.5 M Na_2SO_4) exhibits an active behaviour.

The cathodic portion of the polarization curve for the blank solution is a composite and represents oxygen reduction. For the steel modified by ACE for 12 and 24 h, the corrosion potential values are 0.450 and 0.440 V. While the assembly time was further extended to 48 h and 72 h, the value of corrosion potential did not change. As the exposure time increased from 12 h to 72 h, the corrosion current density of the steel decreased from $6.5 \cdot 10^{-5}$ A cm^{-2} to $1.5 \cdot 10^{-5}$ A cm^{-2}. According to Table 4 and Figure 2, it is clear that the E_{corr} values shifted toward less negative potentials and the I_{corr} values decreased in the samples modified by ACE for 12 to 72 h in comparison with blank sample. The lowest corrosion current density was obtained after 48 to 72 h of time film-forming. This means that the corrosion action noticeably decreases for these films. Given that the displacement in E_{corr} values for the mild steel with the film formed after 12, 24, 48 and 72 h in the vapour phase of ACE is less than ±20 mV with respect to the blank solution, ACE was seen to behave as a mixed-type inhibitor under a cathodic controlled process. Both anodic and cathodic reactions are drastically inhibited after 48 h of exposure to film formation. Both the cathodic slopes and the anodic slopes (Tafel coefficients) do not change obviously, which indicates that the mechanism of the corrosion reaction does not change and the corrosion reaction is inhibited by a simple adsorption mode. This reveals that the inhibitors decrease the corrosion current and thus reduce the corrosion rate. The inhibitive effect of the volatile compounds of the extract on these reactions appeared to be more pronounced at longer exposure times.

The results obtained from weight loss and potentiodynamic polarization are in good agreement, and the compounds inhibition action could also be evidenced by surface SEM images.

SEM analysis

Figure 3*(a)* illustrates the SEM image of a polished steel surface which appeared uniform with scratches and some nicks spread over its surface. This could be due to surface pretreatment with different grades of emery papers and retains the polished sample surface.

Figure 2. Potentiodynamic polarization curves of mild steel in 0.5 M Na_2SO_4 without (the blank sample) and with the film formed after 12, 24, 48 and 72 h in the vapour phase of ACE.

Table 4

**Characteristics of the polarization curves of mild steel in 0.5 M Na_2SO_4
after the formation of protective film from the vapour phase of ACE.**

Film-forming time, h	E_{corr} vs SCE, V	Tafel coefficients, V		I_{corr}, A cm^{-2} 10^{-5}
		b_a	b_c	
0	-0.460	0.10	0.15	13.6
12	-0.450	0.10	0.15	6.5
24	-0.440	0.10	0.15	5.4
48	-0.440	0.10	0.16	2.8
72	-0.440	0.10	0.16	1.5

On the other hand, ACE modified steel surface (Figure 3*(b-d)*) seemed like a smooth surface with the dense organic layer, indicating the successful assembly of ACE SAL over steel surface. It indicates that the API molecules on steel surface have attained a saturated state after the self-assembling time of 48 h. The obtained results indicate that the suitable assembly time is 48 h for the successful formation of SAL with maximum surface coverage. The results indicate that the longer the treatment, the more compact the SALs become, and that the so formed surface layers can inhibit the initiation and the propagation of corrosion process, thus preventing corrosion of the samples.

The surface morphology of the bare steel *(a)* and steel surface covered by ACE SAL during 40 h *(b)*, 48 h *(c)* and after 504 h exposure in conditions of periodic condensation of moisture were studied by SEM and are represented in Figure 4. Bare steel surface after exposure in conditions of periodic condensation of moisture was severely deteriorated and the rough surface is due to the steel dissolution in the corrosive environment (Figure 4*(a)*). Compared with the bare sample, the morphology of the surface was distinctly different for the ACE SAL modified steel after immersion in the corrosive environment.

As it can be seen from Figure 4*(b)*, the surface seemed to be of much less corroded morphology which reveals that the formed ACE SAL effectively protects the steel in conditions of periodic condensation of moisture.

AFM analysis

The surface topography of the steel samples after 12 and 48 h of film-forming ACE SAL was examined by AFM. This microscopic technique has extensively been used to investigate the surface morphology of the metal surface from micro to nano-level in the study of the effect of inhibitor to protect metal against of corrosion.

Figure 5 shows the 2D and 3D AFM images of steel sample after 24 and 48 h of self-assembly time SALs of ACE. To provide quantitative information on the surface roughness, the 2D surface was analysed (Figure 5*(a)* and *(c)*). For the surface in Figure 5*(a)*, it is found to be in the range of 123.073–195.430 nm while root mean square average R_z is between 629.31–809.10 nm.
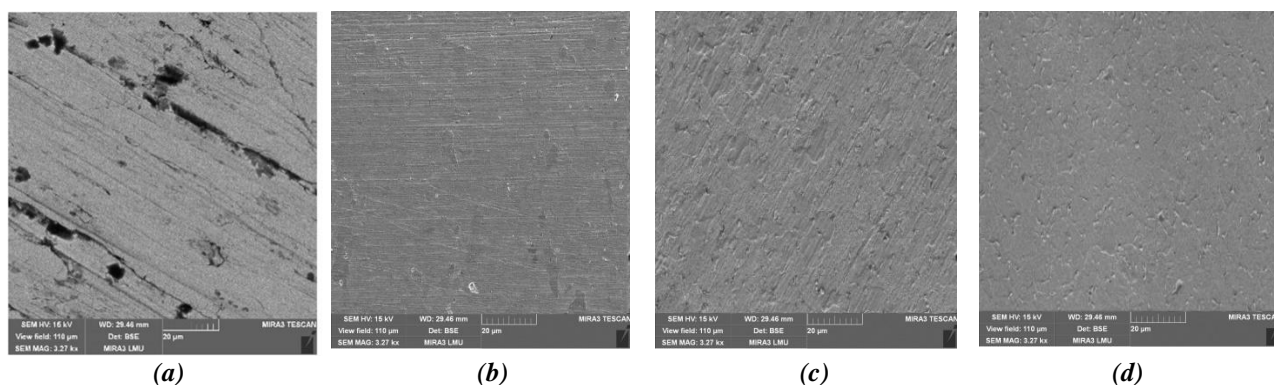

| *(a)* | *(b)* | *(c)* | *(d)* |

Figure 3. SEM images of polished steel *(a)* and ACE SAL modified steel after 24 h *(b)*, 40 h *(c)*, and 48 h *(d)*.
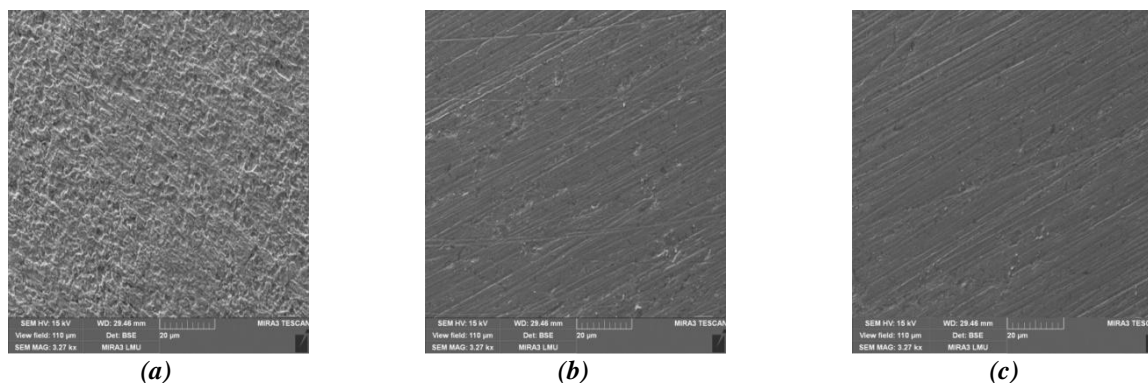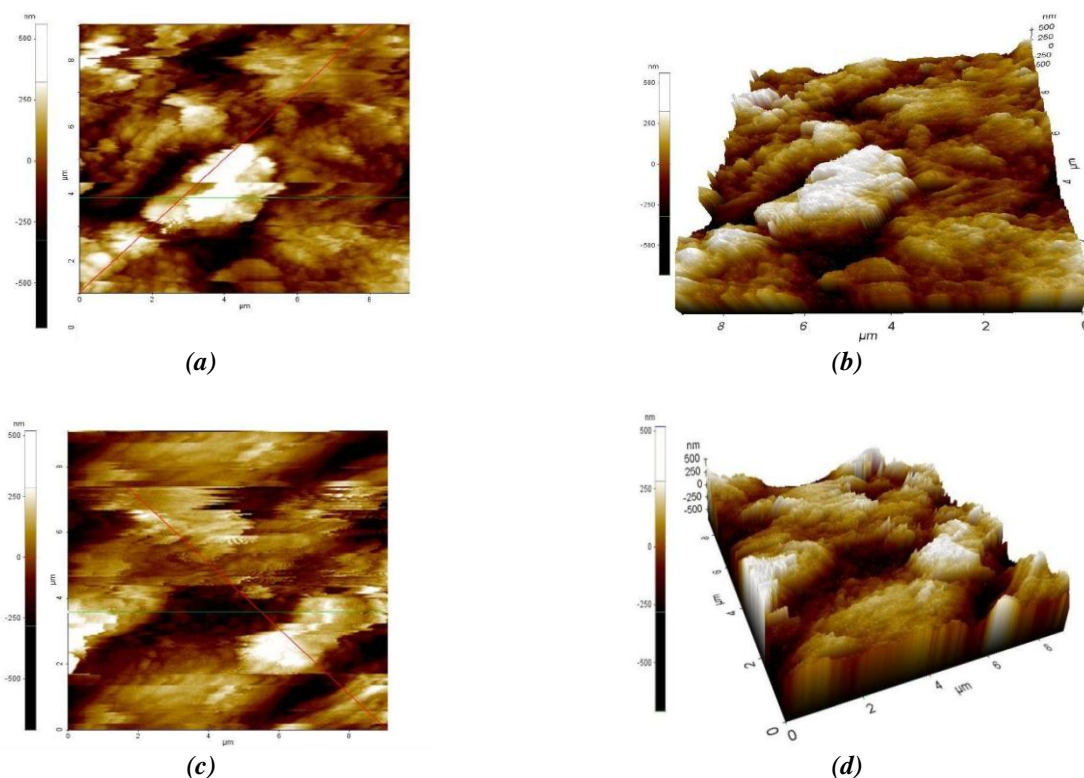

| *(a)* | *(b)* | *(c)* |

Figure 4. SEM images of polished steel *(a)* and after 40 h *(b)*, 48 h *(c)* of film-forming period ACE SAL on steel strips and exposure in conditions of periodic condensation of moisture for 504 h.

(a)

(b)

(c)

(d)

**Figure 5. The 2D and respectively 3D AFM images of steel after 12 h *(a), (b)* and
48 h *(c), (d)* of film-forming ACE SAL on steel strips.**

For the surface modified 48 h (Figure 5*(c)*), the average surface roughness R_a value is in the range of 104.753–171.345 nm and R_z range between 510.852–580.900 nm. R_a gives the mean of a set of individual measurement of surface bands and valleys while R_z gives the RMS (root mean square average) of profile height deviations from mean line. The results obtained by both SEM and AFM show that the formed film becomes denser with the increase of the assembly time.

Due to the complex chemical composition of the ACE, it is difficult to attribute the inhibitive effectiveness to a particular constituent, but it is possible to suppose which type of compound gives a major impact to the inhibition process [32,33]. However, the approach of isolating each component is very cumbersome and takes longer time for investigations. The elucidation of the active compound(s) responsible for corrosion inhibition of ACE has not been reported in the literature yet. This will be the subject of further research.

Conclusions

In the present study, the corrosion inhibition efficiency of the apricot cake extract on the surface of steel has been evaluated. The obtained results from GS-MC measurements revealed that the apricot cake extract contains aldehydes, ketones, and terpene alcohols.

The apricot cake extract has been proved to be an effective inhibitor for the steel corrosion. The molecules from the apricot cake extract formed a compact adsorption layer or self-assembled thin layer-by-layer, which acted as a barrier against steel corrosion. The increase of inhibitor concentration and immersion time led to an increase of surface coverage and corrosion inhibition efficiency. It was found that the maximum corrosion inhibition of about 97% was obtained after 72 h of film-forming.

Electrochemical polarization curves show that the apricot cake extract behaves as the mixed type inhibitor, predominantly of cathodic type. AFM characterization revealed uniform organic coverage on the steel surface. The average roughness value for the steel modified by apricot cake extract is 104.753–171.345 nm. The SEM micrographs showed that the formed apricot cake extract self-assembled layers on steel increased the anticorrosion properties of steel.

References

1. Zhang, D.-Q.; Gao, L.-X.; Zhou, G.-D. Self-assembled urea-amine compound as vapor phase corrosion inhibitor for mild steel. Surface and Coatings Technology, 2010, 204(9-10), pp. 1646-1650.
   DOI: https://doi.org/10.1016/j.surfcoat.2009.10.054

2. Nazeera Banu, V.R.; Rajendran, S.; Senthil Kumaran, S. Investigation of the inhibitive effect of Tween 20 self-assembling nanofilms on corrosion of carbon steel. Journal of Alloys and Compounds, 2016, 675, pp. 139-148.
   DOI: https://doi.org/10.1016/j.jallcom.2016.02.247

3. Qiang, Y.; Fu, S.; Zhang, S.; Chen, S.; Zuo, X. Designing and fabricating of single and double alkyl-chain indazole derivatives self-assembled monolayer for corrosion inhibition of copper. Corrosion Science, 2018, 140, pp. 111-121.
   DOI: https://doi.org/10.1016/j.corsci.2018.06.012

4. Hosseinpour, S.; Göthelid, M.; Leygraf, Ch.; Johnson, M.C. Self-assembled monolayers as inhibitors for the atmospheric corrosion of copper induced by formic acid: a comparison between hexanethiol and hexaneselenol. Journal of the Electrochemical Society, 2014, 161(1), pp. C50-C56.
   DOI: 10.1149/2.056401jes

5. Xu, F.; Yang, J.; Qiu, R.; Hou, J.; Zheng, J.; Zhang, J.; Wang, L.; Sun, Z.; Lin, C. Thiol self-assemble layer as inhibitor to protect B10 from seawater corrosion. Progress in Organic Coatings, 2016, 97, pp. 82-90. DOI: https://doi.org/10.1016/j.porgcoat.2016.03.022

6. Kurniawan, F.; Madurani, K.A. Electrochemical and optical microscopy study of red pepper seed oil corrosion inhibition by self-assembled monolayers (SAM) on 304 SS. Progress in Organic Coatings, 2015, 88, pp. 256-262. DOI: https://doi.org/10.1016/j.porgcoat.2015.07.010

7. Zhang, J.; Liu, Z.; Han, G.-C.; Chen, S.-L.; Chen, Z. Inhibition of copper corrosion by the formation of Schiff base self-assembled monolayers. Applied Surface Science, 2016, 389, pp. 601-608.
   DOI: https://doi.org/10.1016/j.apsusc.2016.07.116

8. Shubha, H.N.; Venkatesha, T.V.; Pavithra, M.K.; Punith Kumar, M.K. Surface modification of mild steel by a self-assembled cetyl-trimethyl ammonium bromide (CTAB) monolayer: Evaluation of its corrosion protection property. Progress in Organic Coatings, 2016, 90, pp. 267-276. DOI: https://doi.org/10.1016/j.porgcoat.2015.10.020

9. Elmi, F.; Gharakhani, A.; Ghasemi, S.; Alinezhad, H. Self-assemble L-glycine and L-cysteine/polydopamine nanohybrid films coated on 304 stainless steel for corrosion study in sterile seawater. Progress in Organic Coatings, 2018, 119, pp. 127-137. DOI: https://doi.org/10.1016/j.porgcoat.2018.01.010

10. Topal, E.; Gece, G. Untangling the inhibition effects of aliphatic amines on silver corrosion: a computational study. Chemistry Journal of Moldova, 2017, 12(2), pp. 64-70.
    DOI: http://dx.doi.org/10.19261/cjm.2017.411

11. Vorobyova, V; Chygyryneś O.; Skiba, M.; Kurmakova, I.; Bondar, O. Self-assembled monoterpenoid phenol as vapor phase atmospheric corrosion inhibitor of carbon steel. International Journal of Corrosion and Scale Inhibition, 2017, 6(4), pp. 485-503.
    DOI: 10.17675/2305-6894-2017-6-4-8

12. Vorob'iova, V.I.; Chyhyrynets, O.E.; Vasyl'kevych, O.I. Mechanism of formation of the protective films on steel by volatile compounds of rapeseed cake. Materials Science, 2015, 50(5), pp. 726-735.
    DOI: https://doi.org/10.1007/s11003-015-9778-z

13. Chyhyrynets, O.E.; Fateev, Yu.F.; Vorobiova, V.I.; Skyba, M.I. Study of the mechanism of action of the isopropanol extract of rapeseed oil cake on the atmospheric corrosion of copper. Materials Science, 2016, 51, pp. 644-651.
    DOI: https://doi.org/10.1007/s11003-016-9886-4

14. Vorobyova, V.; Chygyrynets, O.; Skiba, M. 4-hydroxy-3-methoxybenzaldehyde as a volatile inhibitor on the atmospheric corrosion of carbon steel. Journal of Chemical Technology and Metallurgy, 2018, 53(2), pp. 336-345.
    https://dl.uctm.edu/journal/web/j2018-2

15. Vorobyova, V.; Chygyrynets', O.; Skiba, M.; Zhuk, T.; Kurmakova, I.; Bondar, O. A comprehensive study of grape pomace extract and its active components as effective vapour phase corrosion inhibitor of mild steel. International Journal of Corrosion and Scale Inhibition, 2018, 7(2), pp. 185-202.
    DOI: 10.17675/2305-6894-2018-7-2-6

16. Durainatarajan, P.; Prabakaran, M.; Ramesh, S.; Periasamy, V. Surface protection of copper in 3% NaCl solution by using 1-(n-butyl)imidazole self-assembled monolayer. Materials Today: Proceedings, 2018, 5, 8(3), pp. 16226-16236.
    DOI: https://doi.org/10.1016/j.matpr.2018.05.114

17. Bergsman, D.S.; Liu, T.-L.; Closser, R.G.; Nardi, K.L.; Draeger, N.; Hausmann, D.M.; Bent, S.F. Formation and ripening of self-assembled multilayers from the vapor-phase deposition of dodecanethiol on copper oxide. Chemistry of materials, 2018, 30 (16), pp. 5694-5703.
    DOI: 10.1021/acs.chemmater.8b02150

18. Li, J.; Chen, D.; Zhang, D.; Wang, Y.; Yu, Y.; Gao, L.; Huang, M. Preparation of triazole compounds *via* click chemistry reaction and formation of the protective self-assembled membrane against copper corrosion. Colloids and Surfaces A: Physicochemical and Engineering Aspect, 2018, 550, pp. 145-154.
    DOI: https://doi.org/10.1016/j.colsurfa.2018.04.030

19. Fuchs-Godec, R.; Zerjav, Gr. Corrosion resistance of high-level-hydrophobic layers in combination with Vitamin E–(α-tocopherol) as green inhibitor. Corrosion Science, 2015, 97, pp. 7-16.

DOI: https://doi.org/10.1016/j.corsci.2015.03.016

20. Hosseinpour, S.; Forslund, M.; Johnson, M.C.; Pan, J.; Leygraf, Ch. Atmospheric corrosion of Cu, Zn, and Cu-Zn alloys protected by self-assembled monolayers of alkanethiols. Surface Science, 2016, 648, pp. 170-176.
DOI: https://doi.org/10.1016/j.susc.2015.10.045

21. DIN 17100 St37-2 Carbon and high-strength low-alloy steel plate. (in German) https://www.stahlhaus24.com/files/Dat_1.0038_St37-2_S235JR_gewalzt.pdf

22. Johnsen, L.G.; Skou, P.B.; Khakimov, B.; Bro, R. Gas chromatography – mass spectrometry data processing made easy. Journal of Chromatography A, 2017, 1503, pp. 57-64.
DOI: https://doi.org/10.1016/j.chroma.2017.04.052

23. Wagner, C.; Sefkow, M.; Kopka, J. Construction and application of a mass spectral and retention time index database generated from plant GC/EI-TOF-MS metabolite profiles. Phytochemistry, 2003, 62(6), pp. 887-900. DOI: https://doi.org/10.1016/S0031-9422(02)00703-3

24. Stein, S.E. An integrated method for spectrum extraction and compound identification from gas chromatography/mass spectrometry data. Journal of the American Society for Mass Spectrometry, 1999, 10(8), pp. 770-781. DOI: https://doi.org/10.1016/S1044-0305(99)00047-1

25. Horcas, I.; Fernandez, R.; Gomez-Rodriguez, J.M.; Colchero, J.; Gomez-Herrero, J.; Baro, A.M. WSXM: A software for scanning probe microscopy and a tool for nanotechnology. Review of Scientific Instruments, 2007, 78(1), pp. 013705.
DOI: https://doi.org/10.1063/1.2432410

26. Leygraf, Ch.; Wallinder, I.O.; Tidblad, J.; Graedel, T. Atmospheric Corrosion. John Wiley & Sons: New Jersey, 2016, 397 p.
DOI: 10.1002/9781118762134

27. Zhang, D.-Q.; Gao, L.-X.; Zhou, G.-D. Polyamine compound as a volatile corrosion inhibitor for atmospheric corrosion of mild steel. Materials and Corrosion, 2007, 58(8), pp. 594-598.
DOI: https://doi.org/10.1002/maco.200604046

28. Qiang, Y.; Zhang, S.; Tan, B.; Chen, S. Evaluation of Ginkgo leaf extract as an eco-friendly corrosion inhibitor of X70 steel in HCl solution. Corrosion Science, 2018, 133, pp. 6-16.
DOI: https://doi.org/10.1016/j.corsci.2018.01.008

29. Yıldız, R. An electrochemical and theoretical evaluation of 4,6-diamino-2-pyrimidinethiol as a corrosion inhibitor for mild steel in HCl solutions. Corrosion Science, 2015, 90, pp. 544-553.
DOI: https://doi.org/10.1016/j.corsci.2014.10.047

30. Vorobyova, V.; Chygyrynets', O.; Skiba, M.; Trus, I.; Frolenkova, S. Grape pomace extract as green vapor phase corrosion inhibitor. Chemistry and Chemical Technology, 2018, 12(3), pp. 410-418.
DOI: https://doi.org/10.23939/chcht12.03.410

31. Li, X.; Deng, S.; Xie, X.; Fu, H. Inhibition effect of bamboo leaves' extract on steel and zinc in citric acid solution. Corrosion Science, 2014, 87, pp.15-26.
DOI: https://doi.org/10.1016/j.corsci.2014.05.013

32. Singh, A.; Singh, V.K.; Quraishi, M.A. Aqueous extract of kalmegh (*Andrographis paniculata*) leaves as green inhibitor for mild steel in hydrochloric acid solution. International Journal of Corrosion, 2010, 275983, pp. 1-10.
DOI: https://dx.doi.org/10.1155/2010/275983

33. Rajendran, S.; Rathish, J.; Prabha, S.S. Self-assembling nano films on metal surface as corrosion inhibitors. Advanced Materials Proceedings, 2017, 2(9), pp. 596-601.
DOI: 10.5185/amp.2017/650